Supplementary Information

Adaptive Nanotube Networks Enabling Omnidirectionally Deformable Electro-Driven Liquid Crystal Elastomers Towards Artificial Muscles

Jiao Wang[#a,b], *Hao Zhou*[#a], *Yangyang Fa*[a,b], *Wenhao Hou*[a,b], *Tonghui Zhao*[a,b], *Zhiming Hu*[a,b], *Enzheng Shi**[a], *Jiu-an Lv**[a,b]

*Correspondence to lvjiuan@westlake.edu.cn; shienzheng@westlake.edu.cn

Contents:

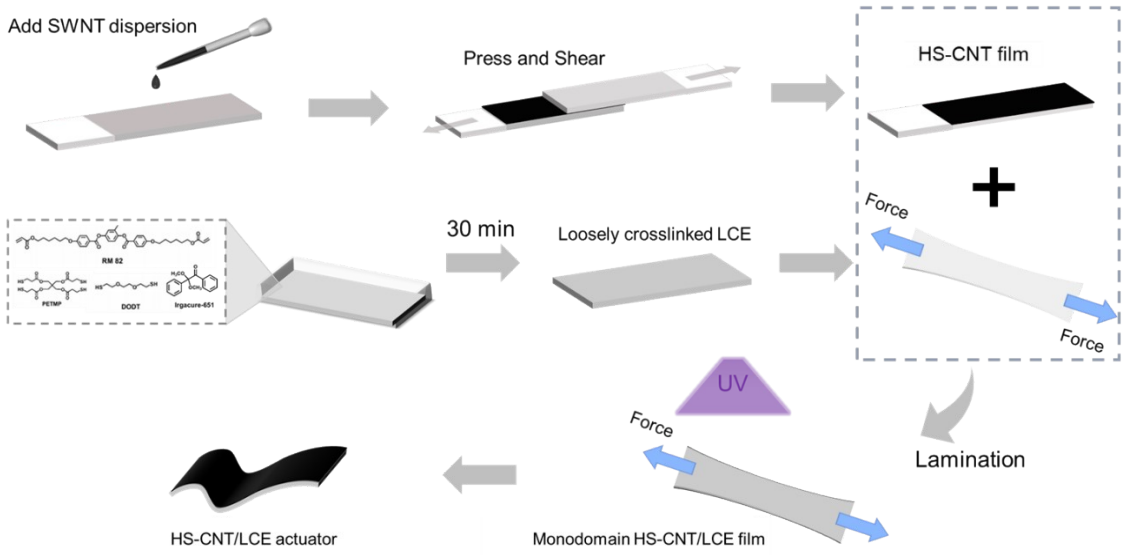

Figure S1. Synthesis of the HS-CNT/LCE actuator.

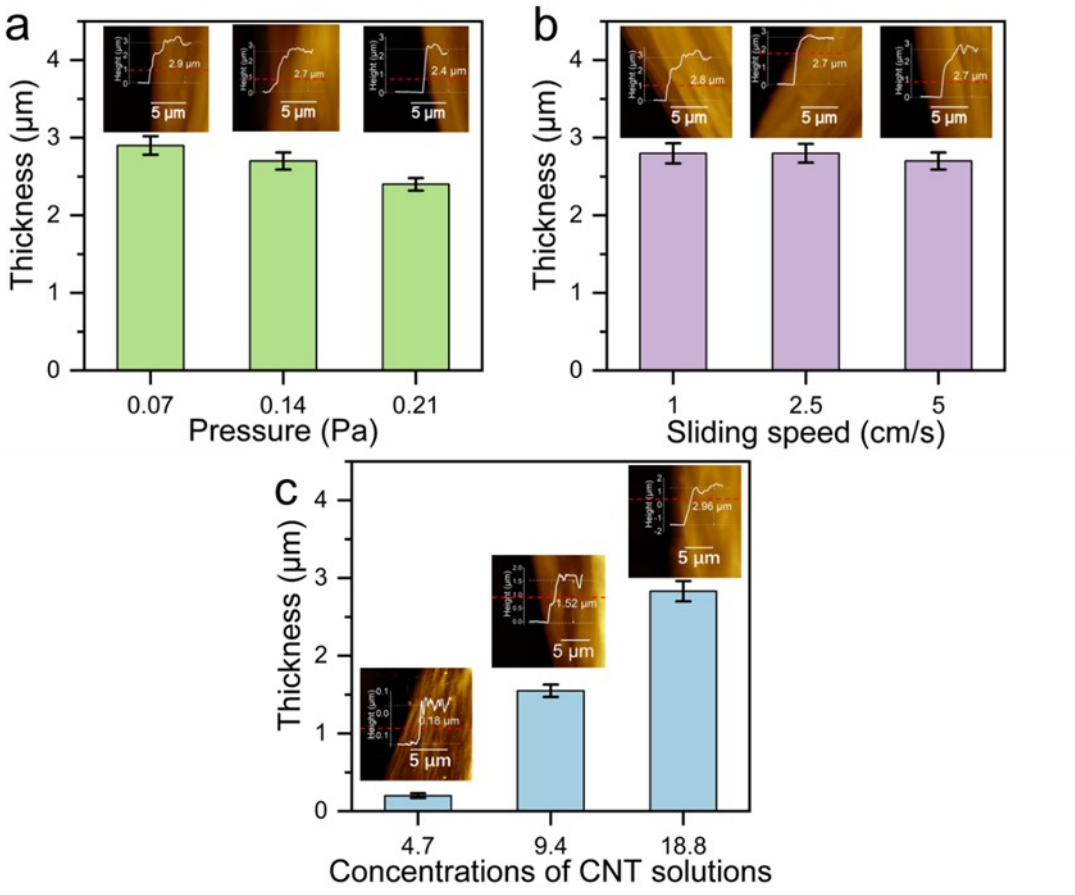

Figure S2. Thickness modulation via applied pressure (a), sliding speed (b) and CNT solutions concentration (c).

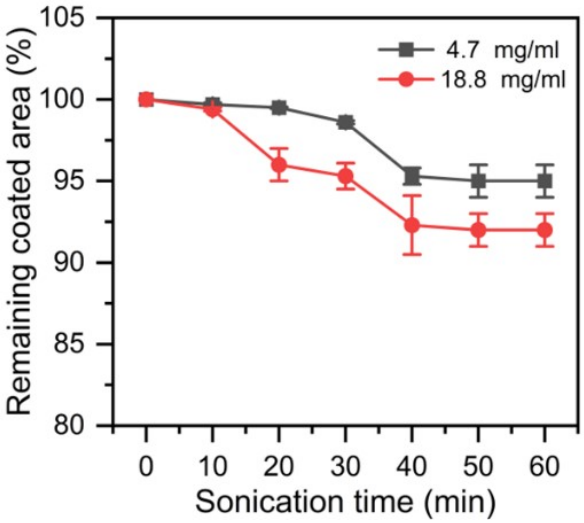

Figure S3. The remaining coated area of HS-CNT film with different density of SWNT after 1h of sonication.

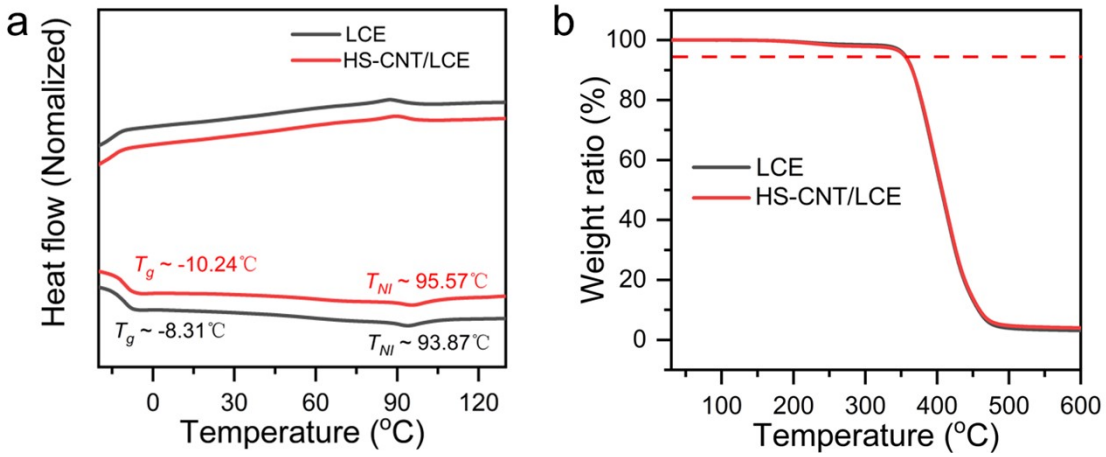

Figure S4. Thermal stability of HS-CNT/LCE (a) DSC curves. (b) TGA curves. Under N_2 atmosphere, the onset temperature of 5 % weight loss was approximately 354 °C.

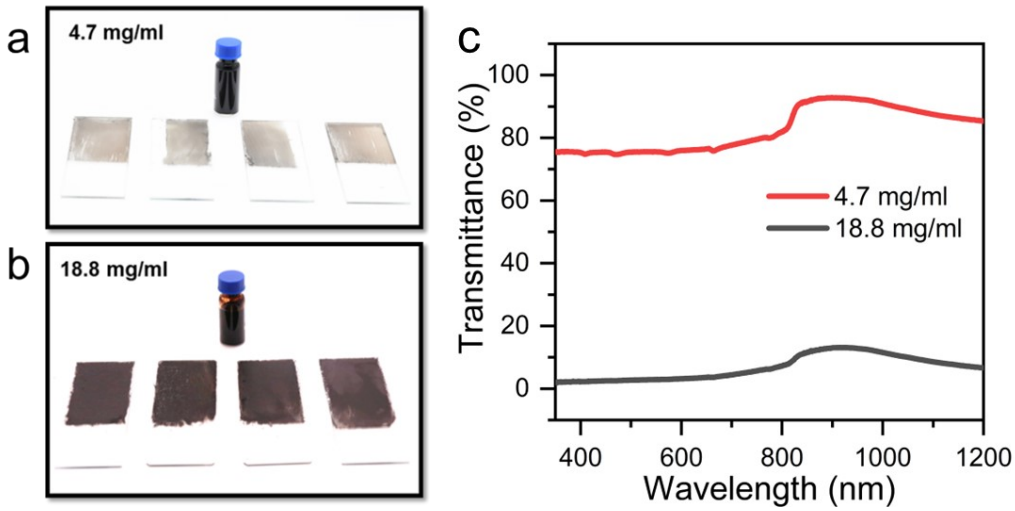

Figure S5. a-b) Photographs of two different concentrations of SWNT dispersions and the corresponding HS-CNT films. c) The transmission spectra of two different concentrations of HS-CNT films.

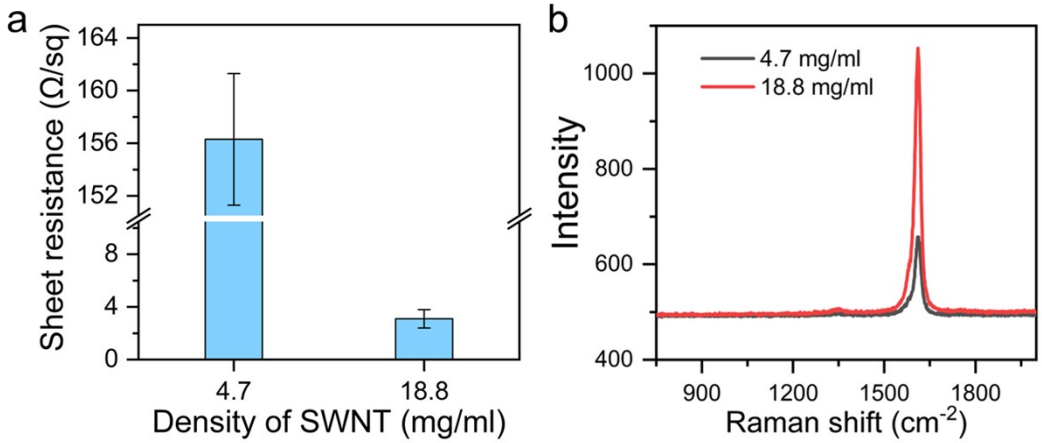

Figure S6. The sheet resistance (a) and Raman spectroscopy (b) of two different concentrations of HS-CNT films.

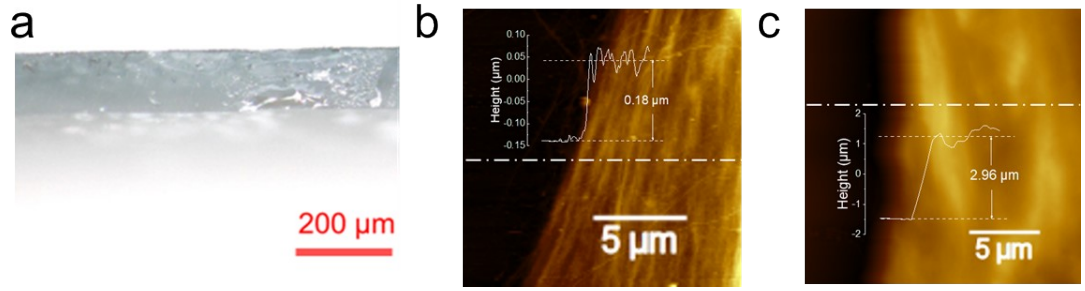

Figure S7. Optical Photographs and atomic force microscopic (AFM) image showing the surface topography and thickness of the LCE and HS-CNT film. a) LCE. b) HS-CNT (4.7 mg/ml). c) HS-CNT (18.8 mg/ml).

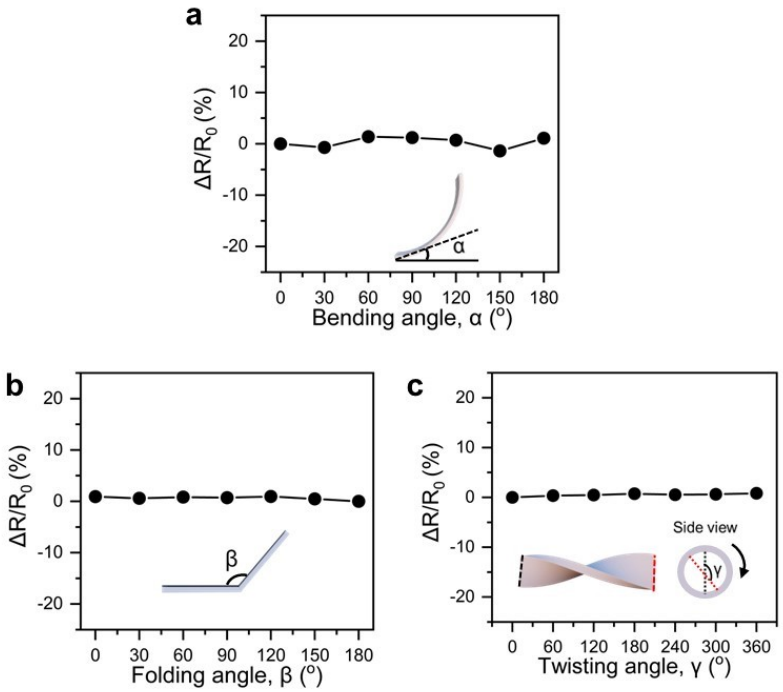

Figure S8. Relative rates of change of resistance of HS-CNT@LCE upon bending (a), folding (b), and twisting (c). The insets schematically show the corresponding deformation mode.

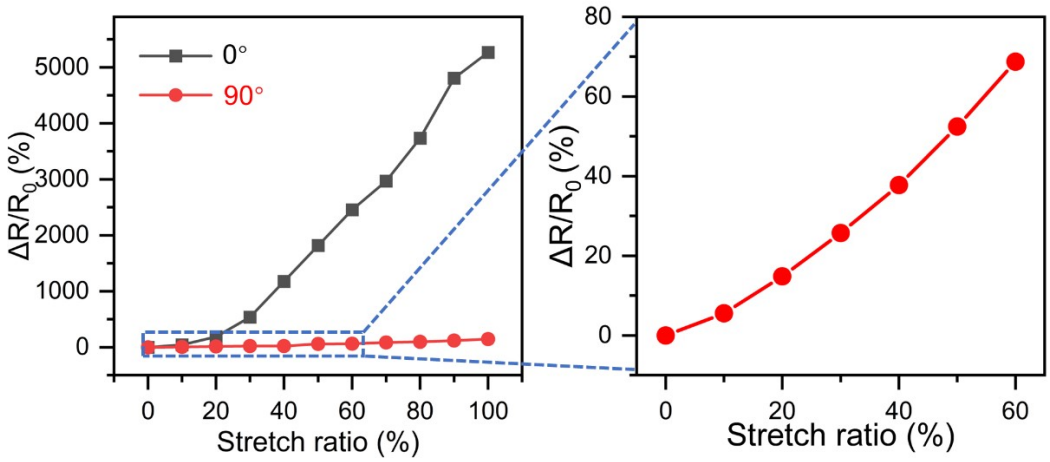

Figure S9. The resistance changes of HS-CNT film (4.7 mg/ml) under various stretching ratio.

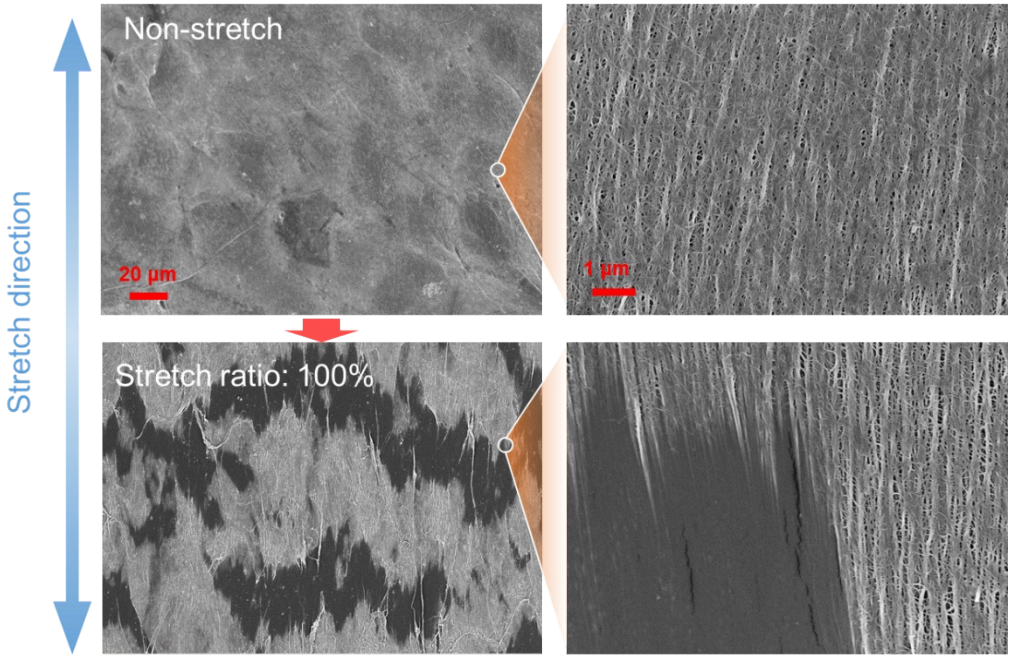

Figure S10. The surface microstructural changes of HS-CNT film (4.7 mg/ml) before and after 100 % stretching along the shear direction obtained by a SEM.

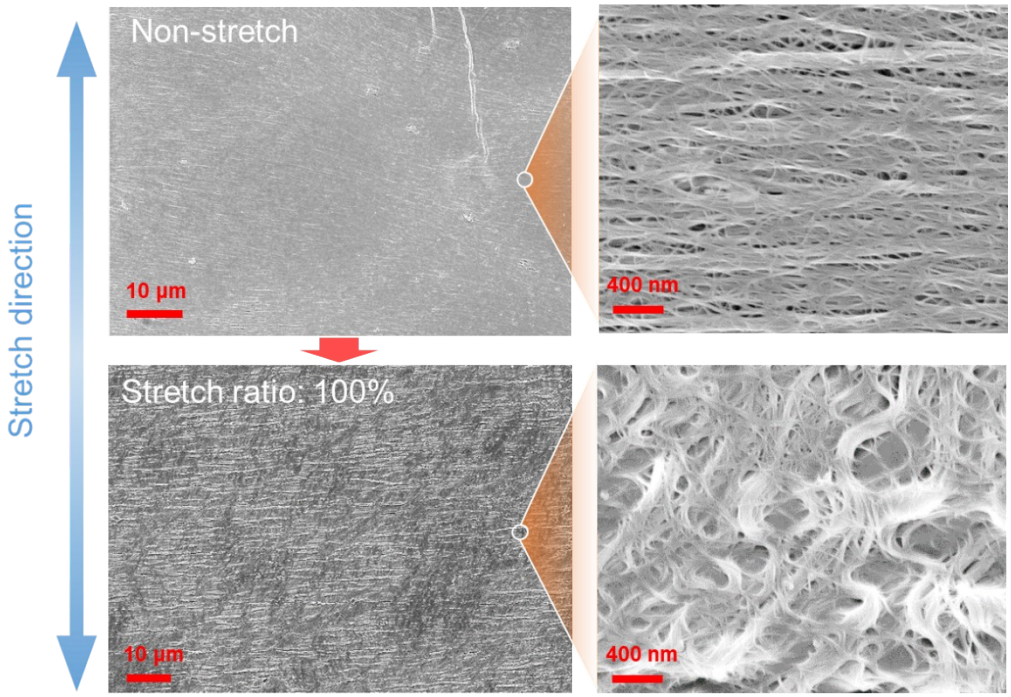

Figure S11. The surface microstructural changes of HS-CNT film (4.7 mg/ml) before and after 100 % stretching perpendicular the shear direction obtained by a SEM.

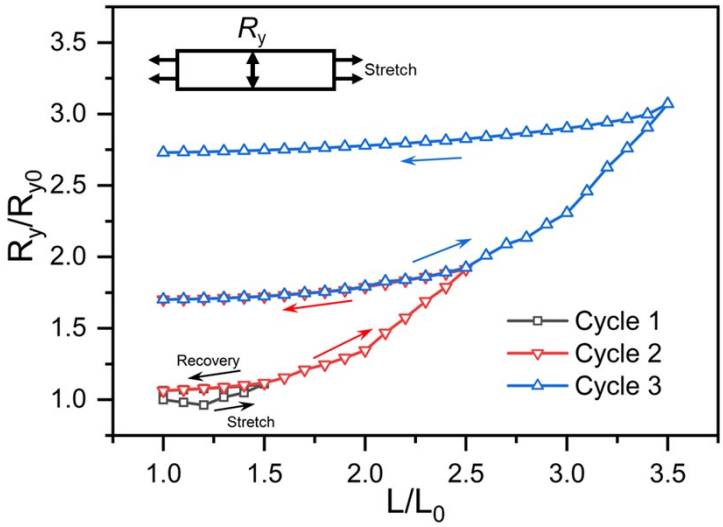

Figure S12. Resistance changes of HS-CNT film (18.8 mg/ml) as a function of strain under a cyclical loading. Experimental results of the resistance change in the stretching angles (90°) under three sequentially increasing strain cycles.

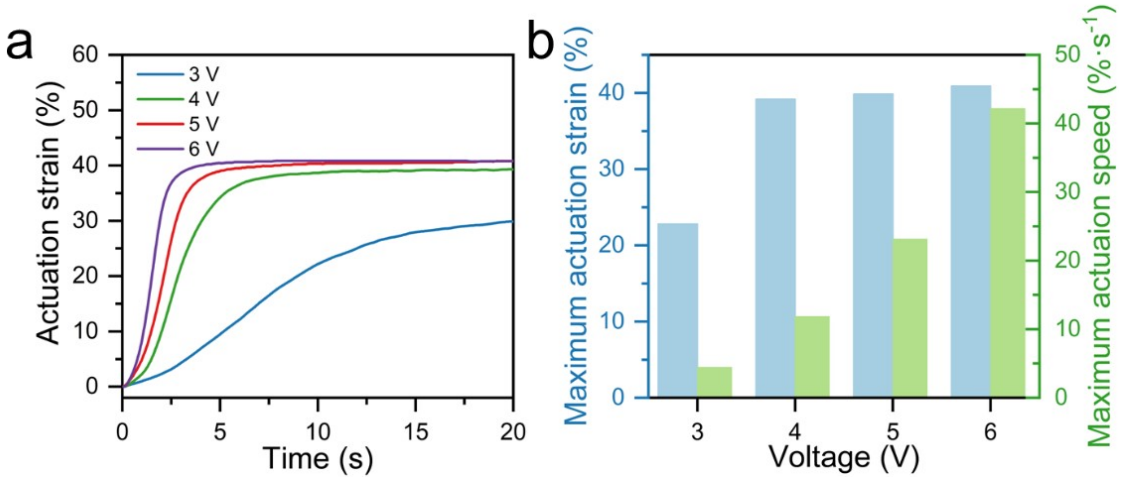

Figure S13. Influences of the applied voltage on actuating strain and speed generated in the HS-CNT/LCE artificial muscle.

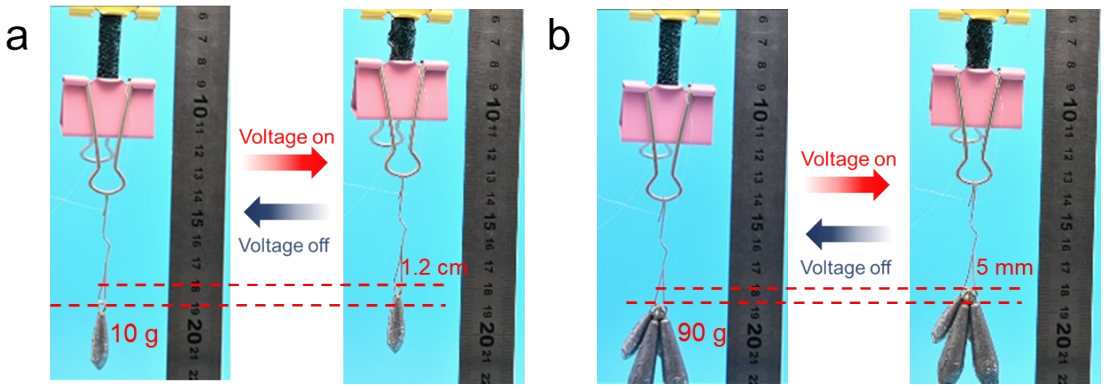

Figure S14. Photograph of single HS-CNT/LCE artificial muscle lifting objects at a voltage of 4 V. a) 10 g. b) 90 g.

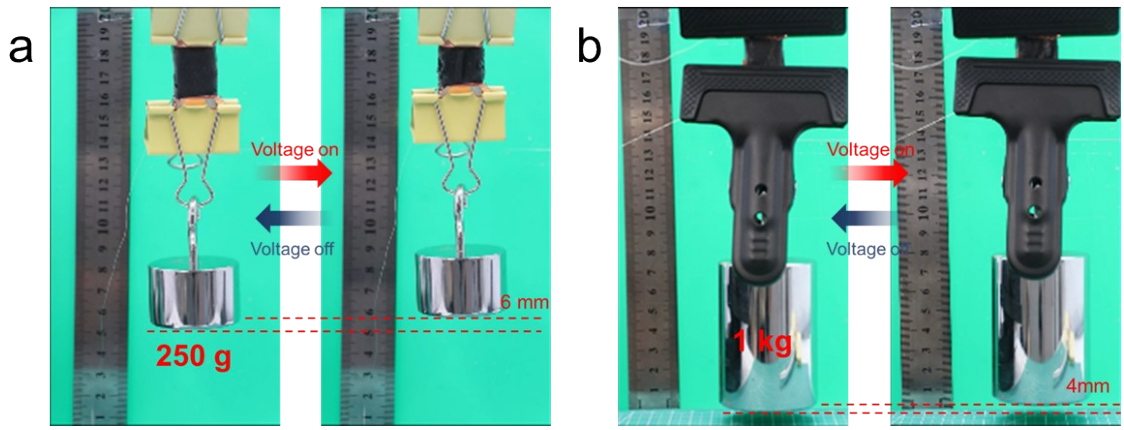

Figure S15. Photograph of multiple HS-CNT/LCE artificial muscles lifting objects at a voltage of 4 V. a) 4 layers, 250 g. b) 10 layers, 1 kg.

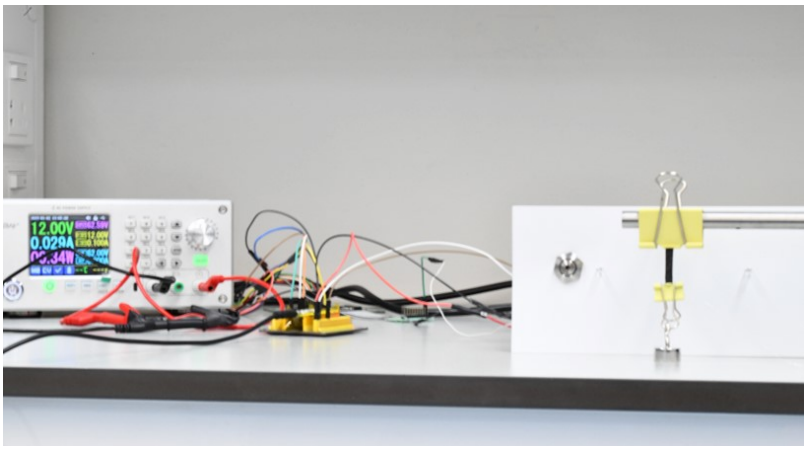

Figure S16. Photograph of closed-loop control artificial muscle system based on HS-CNT/LCE actuator.

Figure S17. Photograph of HS-CNT/LCE actuator with different stretch ratios corresponding to different weights of hanging objects.

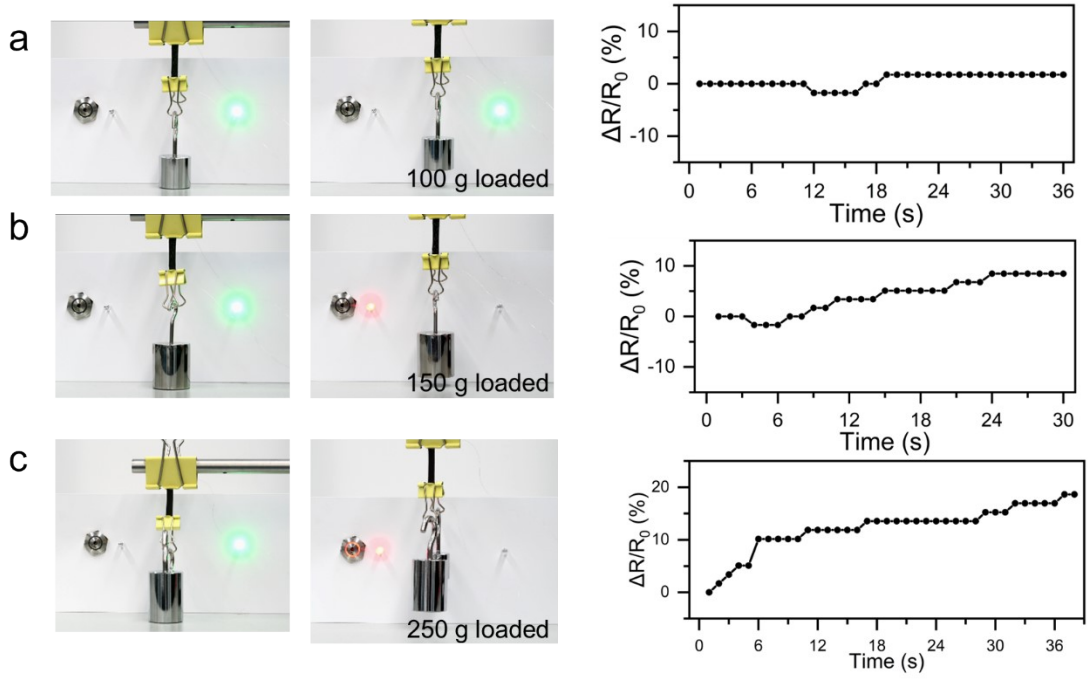

Figure S18. Photograph of HS-CNT/LCE actuator hung with different weights of objects and warning element, and corresponding resistance changing curve during the stretching process in the system. a) 100g. b) 150g. c) 250g.

Table S1. The electromechanical performance comparison of this work with related literatures of LCE based actuators.

Conductive Materials	Driving voltage (V)	Actuation Strain (MPa)	Actuation Strain (%)	Actuation rate (%·s^{-1})	Resistance Change@ actuation strain	Resistance Change@ stretch strain	Ref.
AgNW/MWCNT	6.5	0.46	Bending actuation due to limited deformation		-	-	1
Liquid Metal	2.5	-			-	-	2
CB	50	-			-	-	3
Liquid Metal	1.6	-	11	0.38	-	-	4
Au	30	2.75	45	750	-	R/R0＝4@40%	5
copper wires	3	-	30	1.3	-	-	6
Liquid Metal	15	-	40	284	$\Delta R/R_0$ =2 %@40 %	-	7
helical metal wire	20	0.45	40	1.6	$\Delta R/R_0$ =1.2 %@40 %	-	8
HS-CNT	4	1.1	40	4	$\Delta R/R_0$ =2 %@40 %	R/R_0 = 1.15@100 %	This work

[1] Liu, H. R.; Tian, H. M.; Shao, J. Y.; Wang, Z. J.; Li, X. M.; Wang, C. H.; Chen, X. L. An electrically actuated soft artificial muscle based on a high-performance flexible electrothermal film and liquid-crystal elastomer. ACS Appl. Mater. Interfaces **2020**, 12, 56338-56349.

[2] Ma, B.; Xu, C. T.; Cui, L. S.; Zhao, C.; Liu, H. Magnetic printing of liquid metal for perceptive soft actuators with embodied intelligence. ACS Appl. Mater. Interfaces **2021**, 13, 5574-5582.

[3] Wang, M.; Cheng, Z. W.; Zuo, B.; Chen, X. M.; Huang, S.; Yang, H. Liquid crystal elastomer electric locomotives. ACS Macro Lett. **2020**, 9, 860-865.

[4] Ambulo, C. P.; Ford, M. J.; Searles, K.; Majidi, C.; Ware, T. H. 4D-Printable liquid metal–liquid crystal elastomer composites. ACS Appl. Mater. Interfaces **2020**, 13, 12805-12813.

[5] Wang, Y.; He, Q. G.; Wang, Z. J.; Zhang, S.; Li, C. H.; Wang, Z. J.; Park, Y. L.; Cai, S. Q. Liquid Crystal Elastomer Based Dexterous Artificial Motor Unit. Adv. Mater. **2023**, 35, 2211283.

[6] He, Q. G.; Wang, Z. J.; Wang, Y.; Minori, A.; Tolley, M. T.; Cai, S. Q. Electrically controlled liquid crystal elastomer–based soft tubular actuator with multimodal actuation. Sci. Adv. **2019**, 5, eaax5746.

[7] Sun, J. H.; Wang, Y. P.; Liao, W.; Yang, Z. Q. Ultrafast, High-Contractile Electrothermal-Driven Liquid Crystal Elastomer Fibers towards Artificial Muscles. Small **2021**, 17, 2103700.

[8] Zhao, L. M.; Tian, H. M.; Liu, H. R.; Zhang, W. T.; Zhao, F. B.; Song, X. W.; Shao, J. Y. Bio-Inspired Soft-Rigid Hybrid Smart Artificial Muscle Based on Liquid Crystal Elastomer and Helical Metal Wire. Small **2023**, 19, 2206342.

Captions for Supporting Movies

Movie S1. The actuation process of HS-CNT/LCE film under a voltage of 4 V. The

HS-CNT/LCE film dimensions: 2 cm * 0.6 cm * 150 μm.

Movie S2. HS-CNT/LCE as artificial muscles on a human skeleton.
An HS-CNT/LCE film (1.8 cm * 0.6 cm * 150 μm) was used for artificial masseter muscle. When the voltage was applied, it rapidly contracted, driving the jaw closed. Moreover, a film (6 cm * 0.6 cm * 150 μm) was fixed on the upper limbs of the skeleton model to serve as the biceps artificial muscle. The biceps artificial muscle quickly contracted to pull the arm to bend at the elbow, which enables mimicking the human action of lifting a heavy object by bending the arm. Similarly, artificial triceps femoris prepared by a composite film (3.5 cm * 0.6 cm * 150 μm) can mimic the body movement of lifting the calf.

Movie S3. The multiple artificial muscles lifting process of 1.17kg weight under a voltage of 4 V. The artificial muscle dimensions: 2 cm * 1.5 cm * 150 μm. The number of HS-CNT/LCE films is 10.

Movie S4. The closed-loop control artificial muscle system based on HS-CNT/LCE film. When R/R_0 is below 1.05, it defaults to a normal state indicated by a green light. If it is stretched to a point ($1.05 < R/R_0 \leq 1.15$), we define it as a warning state indicated by a red light. If the stretching continues and the R/R_0 exceeds 1.15, the HS-CNT/LCE film is in a critical damage state in which the red light remains on continuously, a buzzer will alarm, and the control system will automatically apply a certain voltage at the same time to make artificial muscle contract in order to counteract the excessive stretching that could potentially harm it.